Laboratory Investigation (2018) 98:924–934
https://doi.org/10.1038/s41374-018-0055-2

ARTICLE

Microvascular fractal dimension predicts prognosis and response to chemotherapy in glioblastoma: an automatic image analysis study

Cong Chen[1,2,3] · Zhi-cheng He[1,2] · Yu Shi[1,2] · Wenchao Zhou[4] · Xia Zhang[1,2] · Hua-liang Xiao[5] · Hai-bo Wu[1,2] · Xiao-hong Yao[1,2] · Wan-chun Luo[6] · You-hong Cui[1,2] · Shideng Bao[4] · Hsiang-fu Kung[1,2] · Xiu-wu Bian[1,2] · Yi-fang Ping[1,2]

Received: 22 October 2017 / Revised: 11 February 2018 / Accepted: 13 February 2018 / Published online: 15 May 2018

Abstract

The microvascular profile has been included in the WHO glioma grading criteria. Nevertheless, microvessels in gliomas of the same WHO grade, e.g., WHO IV glioblastoma (GBM), exhibit heterogeneous and polymorphic morphology, whose possible clinical significance remains to be determined. In this study, we employed a fractal geometry-derived parameter, microvascular fractal dimension (mvFD), to quantify microvessel complexity and developed a home-made macro in Image J software to automatically determine mvFD from the microvessel-stained immunohistochemical images of GBM. We found that mvFD effectively quantified the morphological complexity of GBM microvasculature. Furthermore, high mvFD favored the survival of GBM patients as an independent prognostic indicator and predicted a better response to chemotherapy of GBM patients. When investigating the underlying relations between mvFD and tumor growth by deploying Ki67/mvFD as an index for microvasculature-normalized tumor proliferation, we discovered an inverse correlation between mvFD and Ki67/mvFD. Furthermore, mvFD inversely correlated with the expressions of a glycolytic marker, LDHA, which indicated poor prognosis of GBM patients. Conclusively, we developed an automatic approach for mvFD measurement, and demonstrated that mvFD could predict the prognosis and response to chemotherapy of GBM patients.

Introduction

Neovascularization is a hallmark of cancer [1]. Evaluation of tumor vascularization is helpful in assisting tumor diagnosis, predicting patient outcome, and searching for therapeutic targets [2, 3]. For example, microvessel density (MVD) has been reported to predict the clinical outcome and the response to therapy in cancer patients [4, 5].

Glioblastoma (GBM) is highly lethal and accounts for 46.1% of the malignant primary brain and the central nervous system tumors [6]. Histologically, GBM is featured by diverse microvascular morphological patterns such as glomeruloid-like vessels [7]. Besides, heterogeneity in the distribution of microvessels among GBMs has been observed [7, 8]. Therefore, the morphological complexity of

Electronic supplementary material The online version of this article (https://doi.org/10.1038/s41374-018-0055-2) contains supplementary material, which is available to authorized users.

✉ Hsiang-fu Kung
hkung@cuhk.edu.hk

✉ Xiu-wu Bian
bianxiuwu@263.net

✉ Yi-fang Ping
pingyifang@126.com

[1] Institute of Pathology and Southwest Cancer Center, Southwest Hospital, Third Military Medical University (Army Medical University), 400038 Chongqing, China

[2] Key Laboratory of Tumor Immunopathology of Ministry of Education of China, Third Military Medical University (Army Medical University), 400038 Chongqing, China

[3] Department of Pathology, 474th Hospital of People's Liberation Army, 830013 Urumqi, China

[4] Department of Stem Cell Biology and Regenerative Medicine, Lerner Research Institute, Cleveland Clinic, Cleveland, Ohio 44195, USA

[5] Department of Pathology, Daping Hospital, Third Military Medical University (Army Medical University), 400042 Chongqing, China

[6] Department of Mathematics, Third Military Medical University (Army Medical University), 400038 Chongqing, China

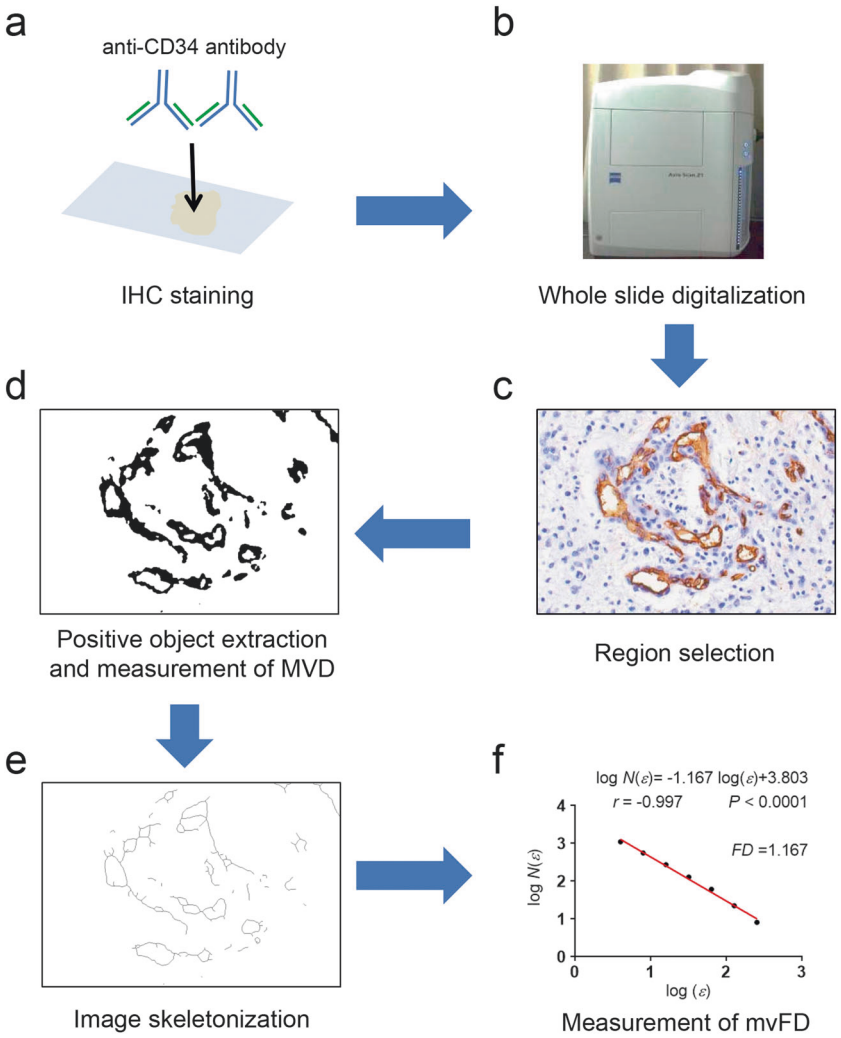

Fig. 1 The workflow for acquisition of tumor microvascular morphometric parameters. **a** IHC staining with anti-CD34 antibody. **b** Whole-slide digitalization. **c** Region selection (a portion of a representative image in order to show the vessel details). **d** Positive object extraction and measurement of MVD. **e** Image skeletonization. **f** Measurement of mvFD by box-counting algorithm

GBM microvasculature may show clinical significance. Several studies have demonstrated the prognostic value of the microvascular patterns in GBM by qualitative assessment, which unexpectedly showed obvious inter-observer variation and thus inconsistent prognostic conclusions [9, 10]. These drawbacks in the qualitative assessment emphasize the establishment of a quantitative, software-based, and standardized method to assess the morphological complexity of GBM microvasculature.

Recently, the fractal geometry has been applied to characterize the complexity of a system including biological structures [11–13]. Fractals are objects which have self-similarity in a range of scales. Fractal dimension quantifies how detailed the fractals change within the scales. It is a non-integer dimension reflecting the space-filling capacity of fractals. Since many objects in biology show fractal characteristics, fractal geometry is widely used in morphology-related biomedical studies. For example, fractal dimension is used to characterize the complexities of tumor infiltrative margin, retinal vasculature, and chromatin structure [14–18]. Notably, fractal dimension has been applied to investigate the microvasculature in tumors such as renal cell carcinoma and GBM [19, 20]. In principle, the microvascular fractal dimension (mvFD) characterizes the complexity of the microvasculature by reflecting the density, shape, size, and distribution of the microvessels [21]. However, the prognostic and predictive significances of mvFD in GBM have not been determined.

In this study, we quantified the morphological complexity of GBM microvasculature by developing a home-made macro in Image J software to automatically obtain the mvFD and explored their potentials in predicting the clinical outcome of GBM patients. Furthermore, we explored the possible reasons underlying the clinical significance of mvFD by investigating the associations between mvFD and tumor cell proliferation, as well as glycolysis. We found that mvFD favors the response to chemotherapy, and thus favors prognosis in GBM patients. In addition, mvFD inversely correlates with microvasculature-normalized tumor cell proliferation and glycolysis of GBM. These results

highlight the utility of mvFD in predicting the response to chemotherapy in GBM patients.

Materials and methods

Patients and tumor samples

Two hundred and seven glioma patients including 94 GBM cases from the Department of Neurosurgery, Southwest Hospital, Third Military Medical University (TMMU) between 2006 and 2014 were enrolled into our study. All patients received surgery only, or surgery plus chemotherapy (Temozolomide or Nimustine) and/or radiotherapy, but did not receive any anti-angiogenic agent. Clinicopathological characteristics and follow-up information including overall survival (OS) time and progression-free survival (PFS) time were collected (Supplementary Table 1). Formalin-fixed paraffin-embedded (FFPE) blocks of tumor specimens were prepared as 4 μm-thick sections. Pathological diagnoses of all glioma cases were re-examined independently by three neuropathologists (Bian XW, Ping YF, and Xiao HL), according to the WHO Classification of tumors of the Central Nervous System (2016). All experiments were conducted under the ethical principles in Declaration of Helsinki. The approval for using human specimens was obtained from the Ethics Committee of TMMU. Two public GBM datasets including the Cancer Genome Atlas (TCGA, http://cancergenome.nih.gov/) and the REpository for Molecular BRAin Neoplasia DaTa (REMBRANDT, http://gliovis.bioinfo.cnio.es/) were mined for the clinical information and the gene expression data of *LDHA* and *MKI67* (gene name of Ki67) [22].

Immunohistochemical staining

Immunohistochemical (IHC) staining was conducted following the standard procedures adapted to antibodies' protocols. The primary antibodies are against CD34 (Dako, Glostrup, Denmark), Ki67 (Dako), IDH1 R132H (Maixin Bio, Fuzhou, China), and LDHA (Cell Signaling Technology, Beverly, MA). Visualization was achieved by Dako REAL™ EnVision™ Detection System (Dako). Isotype IgGs were used as negative controls. Ki67 index was quantified as the percentage of Ki67-positive tumor cells counted in five randomly selected microscopic fields at 400× magnification in the sections representing the pathological characteristics. The expression scores of LDHA were semiquantitatively assessed by two neuropathologists (Bian XW and Ping YF), according to the percentage of positive cells and the staining intensity as previously described [23].

Development of a home-made macro to obtain mvFD

The histological slides were scanned using Axio Scan.Z1 microscopy scanner (Carl Zeiss, Germany) with a 200× magnification (Fig. 1a, b). For each case, five regions (2.5 mm^2 per region) with the highest density of microvessels in the tumor area were chosen and saved as 1920×1080 pixel images (Fig. 1c) [24]. Final microvascular morphometric parameters were the average value based on the five regions. Next, we developed a home-made macro in Image J software (ver 1.45s, NIH, Bethesda, MD) to analyze the images and automatically obtain the mvFD value. There were three procedures in the macro. First, positive object extraction was conducted using thresholding method in hue-saturation-brightness (HSB) color space (Fig. 1d). The hue value threshold was 0 to 90 plus 215 to 255. The saturation threshold was from 25 to 255 for most images, while the range from 38 to 255 was set for images with non-specific background staining. The brightness threshold was from 0 to 255 [25]. Then the images were made into binary and de-noised to increase the smoothness of positive objects (Fig. 1d) [26]. Second, the positive objects on the binary images were skeletonized by an inbuilt algorithm in Image J (Fig. 1e) [27]. Third, mvFD was calculated using box-counting algorithm [19]. The box-counting algorithm is based on counting the number of size-fixed boxes filling the skeletonized objects in a box grid superimposed on two-dimensional histological pictures. The algorithm is described in Equation 1:

$$\mathrm{FD} = \lim_{\varepsilon \to 0} \frac{\log N(\varepsilon)}{\log(1/\varepsilon)}, \tag{1}$$

$$\log N(\varepsilon) = -\mathrm{FD} \log(\varepsilon) + c, \tag{2}$$

where FD is fractal dimension, ε is the side length of a box, and N represents the minimum number of non-overlapping boxes required to completely cover the positive objects. As ε increases exponentially with base 2, N decreases exponentially, where the exponent represents FD. To work out the value of FD, the plot of $\log[N(\varepsilon)]$ against $\log(\varepsilon)$ was drawn with base 10, and the linear regression was conducted using the least squares method (Equation 2) (Fig. 1f). Then the opposite value of the curve's slope was equivalent to FD. The range of the box side length ε from 4 to 256 pixels was used as scale window to ensure a self-similar behavior.

MVD is defined as the percentage of total vascular area divided by whole-tumor area [28]. MVD was also calculated in Image J software based on microvessel-extracted images (Fig. 1d).

Table 1 Correlations between the clinicopathological characteristics and mvFD in GBM patients

Characteristics	mvFD ^{high} (n = 53)	mvFD ^{low} (n = 41)	P
Age (years)			
Median (LQ, UQ)	53 (39, 61)	48 (41, 60)	0.504
Gender			
Female	20	14	0.829
Male	33	27	
KPS score			
<80	28	31	0.032*
≥80	25	10	
Predominant tumor location			
Frontal lobe	20	16	0.772
Temporal lobe	19	13	
Occipital lobe	3	1	
Parietal lobe	7	5	
Midline	4	6	
Ki-67 index (%)			
>20	21	14	0.669
≤20	32	27	
IDH1 mutation status			
Wild type	32	42	0.888
Mutant type	9	11	
MVD (%)			
>4	48	16	<0.001**
≤4	5	25	

LQ lower quartile, *UQ* upper quartile, *KPS* Karnofsky performance scale, *IDH1* isocitrate dehydrogenase 1, *MVD* microvessel density
*$P < 0.05$ or **$P < 0.01$ was regarded as statistically significant

Statistical analysis

To compare the differences of mvFD or MVD between the two groups, independent-sample *t*-test or Mann–Whitney *U*-test was used. Fisher's exact test was conducted to analyze the correlations between clinicopathological characteristics with mvFD (Table 1). Linear regression analysis was performed to determine the possible linear correlations between two continuous variables. For survival analyses, Kaplan–Meier curves were plotted and the two-sided log-rank test was conducted. Besides, univariate and multivariate Cox proportional-hazards regression analyses were performed. All statistical analyses were performed by GraphPad Prism (Version 6.01, GraphPad Software, San Diego, CA) or PASW Statistics (Version 18.0.0, SPSS, Chicago, IL). *$P < 0.05$ or **$P < 0.01$ (two-tailed) was considered as statistically significant.

Results

mvFD reflects the morphological complexity and heterogeneity of microvasculature in glioma

Given that MVD mainly reflects the numbers and density of microvessels, we initially determined whether mvFD would be better than MVD in the quantification of microvasculature complexity by comparing MVD and mvFD in selected glioma sections (Supplementary Table 2). The results showed that gliomas with low MVD could have either low or high mvFD values (Fig. 2a, b). Likewise, gliomas with high MVD could have either high or low mvFD values (Fig. 2a, b). Noticeably, compared with tumors bearing simple capillary-like vessels, GBMs with clustering and tortuous microvessels tended to have a higher mvFD value (Fig. 2a, b). These results indicate that mvFD rather than MVD reflects morphological complexity of glioma microvasculature. Furthermore, to investigate the heterogeneity of microvasculature complexity in gliomas, we determined mvFD values in gliomas of different WHO grades. The results showed that high-grade gliomas (WHO grade III and IV) had higher mvFD than low-grade gliomas (WHO grade II) (Fig. 2c), indicating microvessels in high-grade gliomas are more complex. For high-grade gliomas, no significant difference was found between grade III and IV (GBM) in terms of mvFD value (Fig. 2c). For GBM only, the mvFD values showed a large spectrum, ranging from 0.73 to 1.31 (Fig. 2c). These data indicate that the heterogeneity of morphological complexity of microvasculature exists among different gliomas, as well as within GBMs.

mvFD favors prognosis and response to chemotherapy in GBM patients

To determine the potential prognostic value of mvFD in GBM patients, GBM patients were stratified into mvFD-high (>1.06) and mvFD-low (≤1.06) subgroups, with the average value as the cut-off point. The results showed that GBM patients with high mvFD had prolonged PFS and OS when compared with those with low mvFD (Fig. 3a, b). Meanwhile, MVD also favored GBM prognosis, although the efficiency was lower than mvFD (Supplementary Figure 1a, b). Furthermore, univariate and multivariate Cox regression analyses were performed and showed that mvFD but not MVD was an independent prognostic indicator of PFS and OS in GBM patients (Table 2 and Supplementary Table 3).

Patient survival is affected by the response to therapy [29]. Chemotherapy is a conventional treatment for the newly diagnosed GBM patients [30–32]. Since

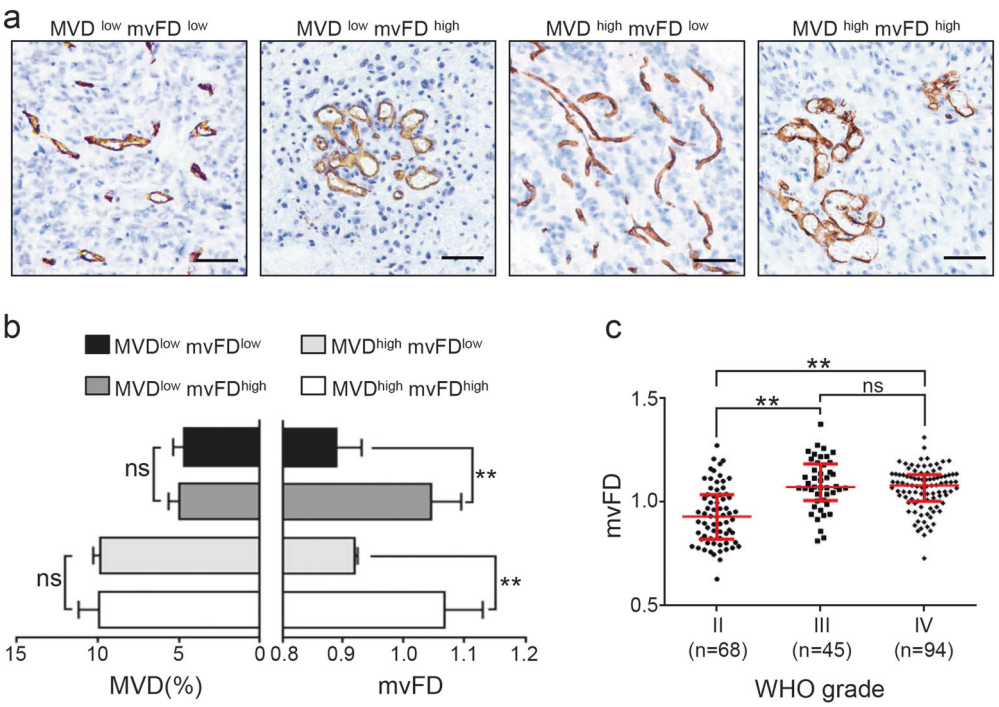

Fig. 2 mvFD reflects the morphological complexity and heterogeneity of the microvasculature in glioma. **a** IHC images stained with anti-CD34 antibody in four groups of gliomas based on the high- or low- values of MVD or mvFD. Scale bars: 50 μm. **b** Comparison of the values of MVD or mvFD in the four groups. Each group has five cases for statistical analysis. **c** Distributions of mvFD values in gliomas with different WHO grades (II, III, and IV). The red horizontal lines indicate median with interquartile range. Data were presented as mean ± SD. Mann–Whitney test was used to assess the statistical significance. The statistical difference is significant when $P < 0.05$ or <0.01. $^{**}P < 0.01$; *ns* not significant

microvasculature provides the routes for chemotherapeutic drugs, we hypothesized that mvFD may affect the response to chemotherapy. Here, we found that high mvFD predicted prolonged PFS and OS in patients who received chemotherapy, while high mvFD showed no predictive value in patients who received no chemotherapy (Fig. 3c, d). Notably, in those patients with low mvFD, chemotherapy seemed to have little effect on their survival (Fig. 3c, d), further emphasizing the role of mvFD in predicting the response to chemotherapy in GBM patients. In addition, linear regression analyses between mvFD and survival time demonstrated that mvFD positively correlated with PFS or OS in patients with chemotherapy (Fig. 3e, f), while no linear correlation was observed between mvFD and PFS or OS in patients without chemotherapy (Fig. 3g, h). In contrast, MVD did not predict different clinical outcomes in patients with or without chemotherapy (Supplementary Figure 1c, d). These data demonstrate that GBM patients with high mvFD are more responsive to chemotherapy. Additionally, we found that the prognostic/predictive value of mvFD was independent of IDH1 mutation, a crucial marker for molecular classification and prognosis in glioblastoma (Table 2 and Supplementary Figure 2a-2i) [33, 34]. Taken together, these results demonstrate mvFD favors prognosis and response to chemotherapy in GBM patients.

mvFD inversely correlates with microvasculature-normalized tumor proliferation

Since mvFD favors GBM response to chemotherapy, we next investigated the underlying reasons. Given that microvasculature constitutes networks to deliver oxygen and nutrition to support tumor cell proliferation, we explored the possible association between mvFD and Ki67 proliferation index. The results showed that mvFD had no correlation with Ki67 in overall GBM patients (Fig. 4a; Table 1). Notably, further analyses showed that mvFD inversely correlated with Ki67 in patients with low mvFD (≤1.06) (Fig. 4b, d), but it had no significant correlation with Ki67 in patients with high mvFD (>1.06) (Fig. 4c). Since microvasculature has promoting effects on tumor proliferation, which would introduce bias especially in the high mvFD patient group, we tried to exclude such influence through normalizing Ki67 by mvFD (Ki67/mvFD), and then explored the relation between mvFD and Ki67/mvFD. In this case, the Ki67/mvFD reflects the microvasculature-independent tumor cell proliferation. The results showed that mvFD had an inverse correlation with Ki67/mvFD in overall GBM patients (Fig. 4e), suggesting that mvFD was inversely associated with microvasculature-independent tumor

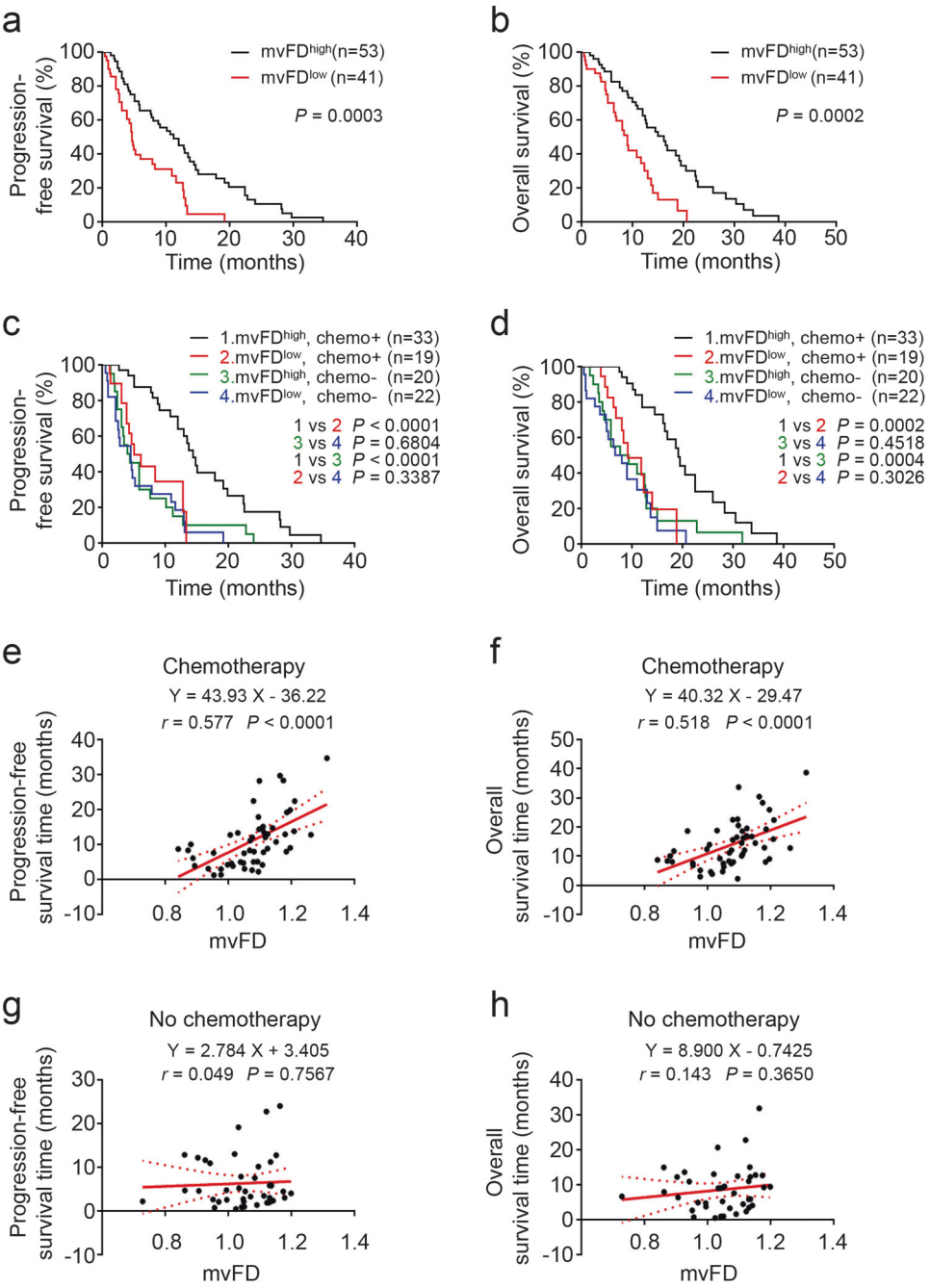

Fig. 3 mvFD favors prognosis and response to chemotherapy in GBM patients. **a**, **b** Kaplan–Meier curves showing the differences of GBM patient survival based on mvFD value. **c**, **d** Kaplan–Meier curves showing the differences of GBM patient survival based on mvFD value and chemotherapy treatment. chemo+, patients received chemotherapy; chemo-, patients did not receive chemotherapy. **a**–**d** Log-rank test was used to obtain the *P*-value with the average value of mvFD in the GBM group used as the cut-off point to discriminate high (>1.06) and low (≤1.06) subgroups. The statistical difference is significant when $P < 0.05$. **e**–**h** Scatter plots and linear regression analyses showing the correlations between mvFD and progression-free survival (**e**, **g**) or overall survival (**f**, **h**) in GBM patients with chemotherapy (**e**, **f**) or without chemotherapy (**g**, **h**). The red straight line in each panel is the best fit line of linear regression. The red dotted lines in each panel are the 95% confidence band of the best fit line. The statistically significant linear regression is indicated when $P < 0.05$. *r*: correlation coefficient

proliferation. Furthermore, we investigated the prognostic values of Ki67/mvFD in GBM, with the average value of Ki67/mvFD in the GBM group as the cut-off point to discriminate high (>21.6) and low (≤21.6) subgroups. The results showed that high Ki67/mvFD predicted shortened PFS and OS in GBM patients (Fig. 4f, g). These data indicate that GBM patients with low mvFD may possess elevated level of microvasculature-independent tumor proliferation that may contribute to poor prognosis and poor response to chemotherapy of GBM patients.

mvFD is inversely associated with the glycolysis status of GBM

Next, we explored the relationship between mvFD and other molecular markers which could reflect microvasculature-independent tumor proliferation. Previous reports suggested that tumor cells utilize glycolysis for proliferation to adapt to a stressful environment, lacking microvessels [35]. Thus glycolysis could be regarded as a parameter for microvasculature-independent tumor proliferation which

Table 2 Multivariate Cox regression analysis in GBM patients

Variable[a]	Progression-free survival			Overall survival		
	HR	95% CI	*P*	HR	95% CI	*P*
IDH1 mutation	0.349	0.157–0.777	0.010*	0.373	0.145–0.964	0.042*
mvFD	0.426	0.241–0.753	0.003**	0.305	0.161–0.577	<0.001**
Ki-67 index	1.783	1.035–3.072	0.037*	1.963	1.102–3.499	0.022*
Extent of surgical resection	0.604	0.366–0.996	0.048*	0.493	0.282–0.863	0.013*
Radiotherapy	0.549	0.303–0.994	0.048*	0.317	0.174–0.580	<0.001**

HR hazard ratio, *CI* confidence interval, *KPS* Karnofsky performance scale

*$P < 0.05$ or **$P < 0.01$ was regarded as statistically significant

[a]Age (1: <50 years vs. 2: ≥50 years), gender (1: male vs. 2: female), KPS score (1: <80 vs. 2: ≥80), extent of surgical resection (1: partial resection vs. 2: gross total resection), chemotherapy (1: No vs. 2: Yes), radiotherapy (1: No vs. 2: Yes), predominant tumor location (1: frontal lobe vs. 2: temporal lobe vs. 3: occipital lobe vs. 4: parietal lobe vs. 5: cerebellum vs. 6: midline), Ki-67 index (1: ≤20% vs. 2: >20%), IDH1 mutation (1: IDH1 wild type vs. 2: IDH1 mutant), mvFD (1: ≤1.06 vs. 2: >1.06), MVD (1: ≤5.28% vs. 2: >5.28%) were included in the analysis. Backward stepwise method was used

was validated by the positive correlations between gene expressions of *LDHA* and *MKI67* (gene name of Ki67) in GBMs of TCGA and REMBRANDT datasets (Fig. 5a, b). *LDHA* encodes Lactate Dehydrogenase A, a key enzyme involved in glycolysis [36]. We then investigated the possible association between mvFD and LDHA expressions by IHC analysis on human primary GBM sections (Fig. 5c). The results showed that LDHA had higher expressions in GBMs with low mvFD than in those with high mvFD (Fig. 5d), implying an inverse correlation between mvFD and glycolysis status of GBM tumor cells. Furthermore, we performed IHC staining to determine LDHA expressions in 56 GBM samples and found that LDHA was a marker for poor prognosis in GBM patients (Fig. 5e, f). Similarly, survival analyses based on *LDHA* mRNA expressions in GBM from TCGA and REMBRANDT databases showed that high *LDHA* level indicated shortened PFS (Fig. 5g) and OS (Fig. 5h, i). Conclusively, mvFD is inversely correlated with glycolysis status in GBM, validating the inverse association between microvasculature complexity and the microvasculature-independent tumor proliferation in GBM.

Discussion

Currently, the software-based automated morphometric analysis in pathology is applied in assessing IHC scores, measuring morphological parameters of microvessels and extracting cell nuclear features [37–40]. These practices assist pathological diagnoses and may exhibit prognostic and predictive values. In this study, fractal dimension, a parameter derived from fractal geometry which could reflect the complexity of fractal structures, was deployed to quantify GBM microvasculature. Preclinical analyses showed that mvFD favored GBM patient prognosis and response to chemotherapy. Notably, mvFD inversely correlated with microvasculature-normalized tumor cell proliferation and glycolysis status of GBM. These findings highlight the roles of microvasculature complexity in predicting the clinical outcome and implicate its relations with tumor cell aggressiveness in GBM.

The microvasculature heterogeneity is a common phenomenon in many tumors and may provide promising biomarkers [41–43]. The microvasculature could reflect the tumor's metabolic dependence for oxygen and nutrients [28]. Several studies have showed the close associations between microvasculature and metabolism in tumors [44, 45]. Since the metabolic demands are heterogenous in all grades of gliomas, it is reasonable to infer that microvasculature of gliomas are heterogenous [44, 46, 47]. In grade II glioma, lower mvFD was observed because the microvessels are simple and capillary-like in morphology and have lower density than the microvessels in high-grade gliomas (grades III and IV). The reason may be that grade II glioma has less metabolic requirements and less angiogenic capability than high-grade gliomas [46, 47].

Our study demonstrated that mvFD showed advantages over MVD in quantification of morphological complexity of glioma microvasculature. Previously, the roles of MVD in GBM prognosis were not consistent among researchers [10]. In fact, MVD doesn't have the capacity to characterize the complicated microvascular morphology in high-grade gliomas which could be achieved by mvFD. Our results demonstrated that mvFD quantified the architecture heterogeneity of microvessels within a GBM tumor and among GBMs which showed implications of its clinical significance.

As we know, the resistance to therapy in GBM is a major obstacle to the treatment efficacy [48, 49]. Therefore, it is crucial to understand the underlying mechanisms and to find the corresponding biomarkers predicting response to therapy. Previous studies have elucidated morphological

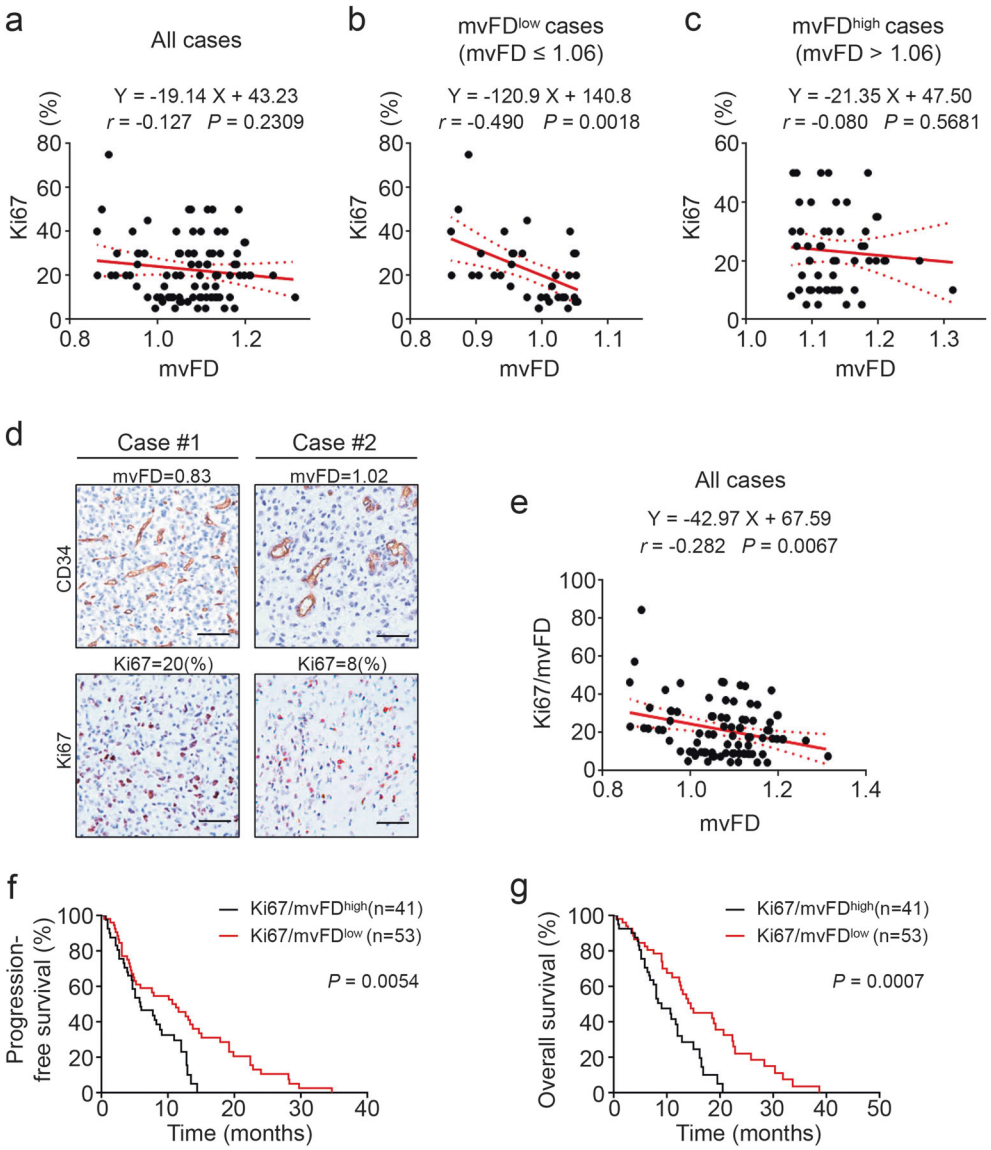

Fig. 4 mvFD inversely correlates with microvasculature-normalized tumor proliferation. **a**–**c** Scatter plots and linear regression analyses showing the correlation between mvFD and Ki67 index. **d** IHC images labeled with anti-CD34 or anti-Ki67 antibody in GBM cases with different mvFD values. Scale bars: 50 μm. **e** Scatter plot and linear regression analysis showing the correlation between mvFD and Ki67/mvFD. **a**–**c**, **e** The red straight line in each panel is the best fit line of linear regression. The red dotted lines in each panel are the 95% confidence band of the best fit line. *r*, correlation coefficient. **f**, **g** Kaplan–Meier curves showing the differences of PFS (**f**) and OS (**g**) of GBM patients based on Ki67/mvFD value. **f**, **g** Log-rank test was used to obtain the *P*-value with the average value of Ki67/mvFD in the GBM group used as the cut-off point to discriminate high (>21.6) and low (≤21.6) subgroups. The statistical difference is significant when $P < 0.05$

markers based on microvessel could act as responders of therapy in cancer [50–52]. For example, Tolaney et al. reported that a high pre-treatment microvascular density predicts better pathologic response to neoadjuvant bevacizumab and chemotherapy in breast cancer patients [50]. In our study, we demonstrated that mvFD predicts better response to chemotherapy in GBMs. Since fractal structure has characteristics of self-organization, we speculate that GBM with a high mvFD value may possess a more extended microvascular network, which could promote drug delivery [53]. More importantly, we found the underlying relations between microvasculature with the tumor cell proliferation as well as glycolysis status of GBM. Like many other cancers, GBM preferentially utilizes glycolysis as a key energy source regardless of oxygen supply, which is also known as "Warburg effect" [54, 55]. The glycolysis in GBM also displays heterogeneity [56]. Some cases have higher levels of glycolysis, thus GBM cells are adapted to the metabolic condition lacking oxygen supply, where glycolysis meets their metabolic demands for growth and

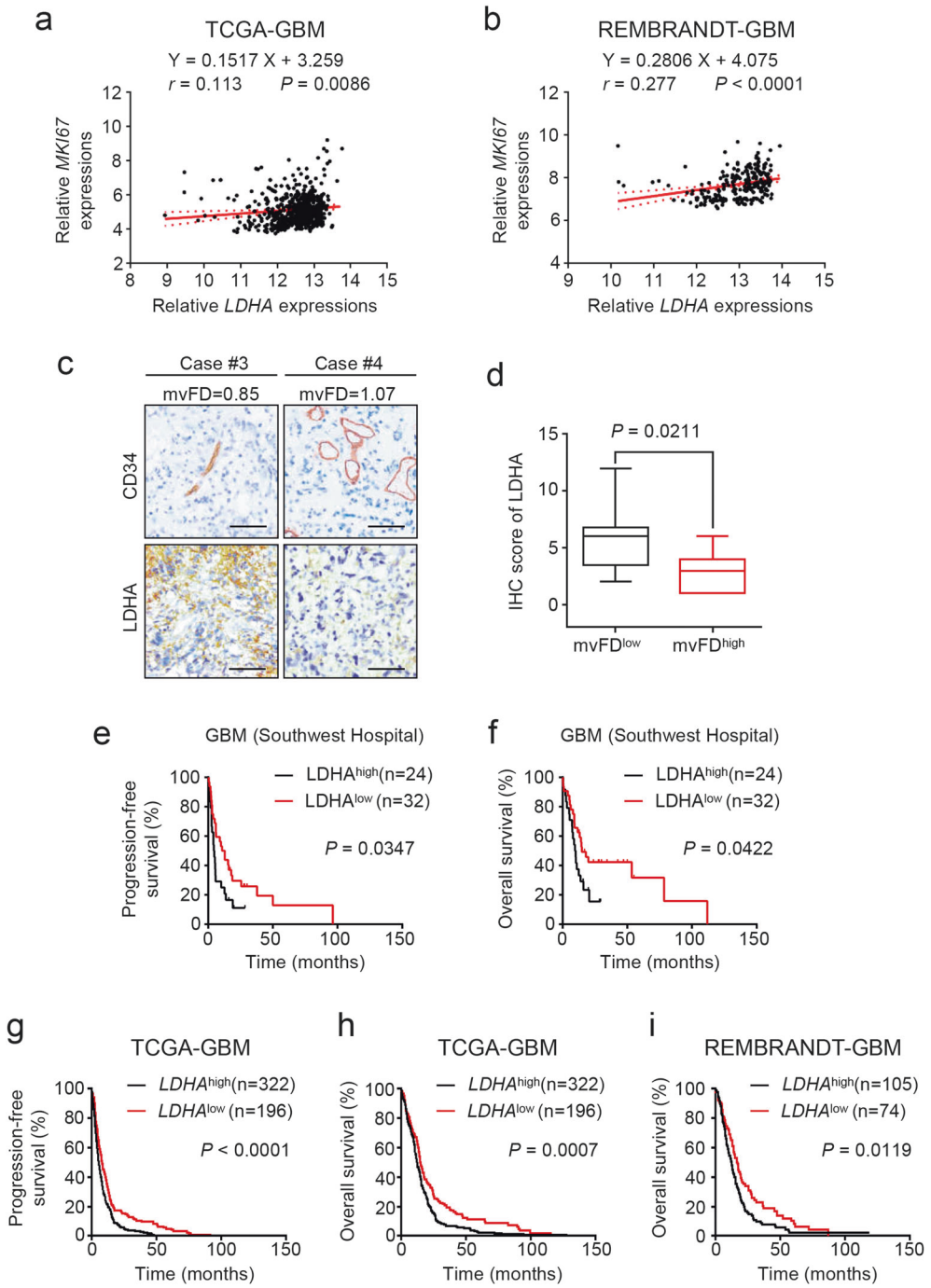

Fig. 5 mvFD is inversely associated with glycolysis status of GBM. **a**, **b** Scatter plots and linear regression analyses showing the correlations between the expressions of *LDHA* and *MKI67* in GBM from TCGA (**a**) and REMBRANDT (**b**) databases. The red straight line in each panel is the best fit line of linear regression. The red dotted lines in each panel are the 95% confidence band of the best fit line. *r*, correlation coefficient. **c** IHC images labeled with anti-CD34 or anti-LDHA antibody in GBM cases with different mvFD values. Scale bars: 50 μm. **d** Comparison of the IHC scores of LDHA expressions in $mvFD^{high}$ GBMs (10 cases) and $mvFD^{low}$ GBMs (10 cases). $mvFD^{high}$: >1.06; $mvFD^{low}$: ≤1.06. Data were presented as mean ± SD. The Mann–Whitney test was used to assess the statistical significance. **e**, **f** Kaplan–Meier curves showing the differences of progression-free survival (**e**) and overall survival (**f**) of GBM patients based on IHC scores of LDHA. **g**–**i** Kaplan–Meier curves showing the differences of GBM patient survival based on *LDHA* mRNA expressions from TCGA (**g**, **h**) and REMBRANDT (**i**) databases. Log-rank test was used for survival analysis with X-tile software used to obtain the cut-off point [60]. For all panels with statistical analyses, $P < 0.05$ is regarded as statistically significant

proliferation [35, 57]. In other words, GBM with higher glycolysis level has less dependence on microvasculature and thus lower mvFD. Furthermore, glycolysis indicates poor prognosis and contributes to tumor resistance to therapies including chemotherapy [58]. As a result, GBM with lower mvFD had higher level of microvasculature-normalized tumor cell proliferation (higher Ki67/mvFD) and higher glycolysis level, thus predicted worse prognosis and worse response to chemotherapy of GBM patients than GBM with higher mvFD.

Taken together, our findings highlight mvFD as a critical morphometric marker favoring prognosis and response to chemotherapy in GBM patients. Its associations with tumor proliferation and metabolic status were also addressed. To investigate the possible clinical significance of mvFD in a broader spectrum, further studies in other solid tumors like breast cancer are required. The potential application of mvFD in evaluating tumor response to anti-angiogenic agents also needs to be investigated. Besides, new strategies should be developed to acquire mvFD based on medical imaging techniques such as time-of-flight magnetic resonance angiography (TOF-MRA) [59]. These techniques are non-invasive and could visualize three-dimensional vasculature, thus may show great potential in monitoring disease progression and response to therapies.

Acknowledgements This project was supported by grants from the National Natural Science Foundation of China (No. 81370071), Society of Neuro-oncology, Chinese Anti-Cancer Association (No.CSNO-2015-MSD08), and Southwest Hospital (No. SWH2016ZDCX3023).

Compliance with ethical standards

Conflict of interest The authors declare that they have no conflict of interest.

References

1. Hanahan D, Weinberg RA. Hallmarks of cancer: the next generation. Cell. 2011;144:646–74.
2. Carmeliet P, Jain RK. Molecular mechanisms and clinical applications of angiogenesis. Nature. 2011;473:298–307.
3. Emblem KE, Mouridsen K, Bjornerud A, et al. Vessel architectural imaging identifies cancer patient responders to anti-angiogenic therapy. Nat Med. 2013;19:1178–83.
4. Uzzan B, Nicolas P, Cucherat M, et al. Microvessel density as a prognostic factor in women with breast cancer: a systematic review of the literature and meta-analysis. Cancer Res. 2004;64:2941–55.
5. Eefsen RL, Engelholm L, Willemoe GL, et al. Microvessel density and endothelial cell proliferation levels in colorectal liver metastases from patients given neo-adjuvant cytotoxic chemotherapy and bevacizumab. Int J Cancer. 2016;138:1777–84.
6. Ostrom QT, Gittleman H, Fulop J, et al. CBTRUS statistical report: primary brain and central nervous system tumors diagnosed in the United States in 2008–2012. Neuro Oncol. 2015;17: iv1–62.
7. Folkerth RD. Descriptive analysis and quantification of angiogenesis in human brain tumors. J Neurooncol. 2000;50:165–72.
8. Bian XW, Wang QL, Xiao HL, et al. tumor microvascular architecture phenotype (T-MAP) as a new concept for studies of angiogenesis and oncology. J Neurooncol. 2006;80:211–3.
9. Birner P, Piribauer M, Fischer I, et al. Vascular patterns in glioblastoma influence clinical outcome and associate with variable expression of angiogenic proteins: evidence for distinct angiogenic subtypes. Brain Pathol. 2003;13:133–43.
10. Preusser M, Heinzl H, Gelpi E, et al. Histopathologic assessment of hot-spot microvessel density and vascular patterns in glioblastoma: poor observer agreement limits clinical utility as prognostic factors: a translational research project of the European Organization for Research and Treatment of Cancer Brain tumor Group. Cancer. 2006;107:162–70.
11. Mandelbrot BB. The fractal geometry of nature. New York: W. H. Freeman and Co., 1982.
12. West GB, Brown JH, Enquist BJ. The fourth dimension of life: fractal geometry and allometric scaling of organisms. Science. 1999;284:1677–9.
13. Lennon FE, Cianci GC, Cipriani NA, et al. Lung cancer-a fractal viewpoint. Nat Rev Clin Oncol. 2015;12:664–75.
14. Nyirenda N, Farkas DL, Ramanujan VK. Preclinical evaluation of nuclear morphometry and tissue topology for breast carcinoma detection and margin assessment. Breast Cancer Res Treat. 2011;126:345–54.
15. Laughney AM, Krishnaswamy V, Rizzo EJ, et al. Scatter spectroscopic imaging distinguishes between breast pathologies in tissues relevant to surgical margin assessment. Clin Cancer Res. 2012;18:6315–25.
16. Grauslund J, Green A, Kawasaki R, et al. Retinal vascular fractals and microvascular and macrovascular complications in type 1 diabetes. Ophthalmology. 2010;117:1400–5.
17. Lieberman-Aiden E, van Berkum NL, Williams L, et al. Comprehensive mapping of long-range interactions reveals folding principles of the human genome. Science. 2009;326:289–93.
18. Barbieri M, Chotalia M, Fraser J, et al. Complexity of chromatin folding is captured by the strings and binders switch model. Proc Natl Acad Sci USA. 2012;109:16173–8.
19. Sabo E, Boltenko A, Sova Y, et al. Microscopic analysis and significance of vascular architectural complexity in renal cell carcinoma. Clin Cancer Res. 2001;7:533–7.
20. Di Ieva A, Grizzi F, Sherif C, et al. Angioarchitectural heterogeneity in human glioblastoma multiforme: a fractal-based histopathological assessment. Microvasc Res. 2011;81:222–30.
21. Di Ieva A, Grizzi F, Tschabitscher M, et al. Correlation of microvascular fractal dimension with positron emission tomography [(11)C]-methionine uptake in glioblastoma multiforme: preliminary findings. Microvasc Res. 2010;80:267–73.
22. Bowman RL, Wang Q, Carro A, et al. GlioVis data portal for visualization and analysis of brain tumor expression datasets. Neuro Oncol. 2017;19:139–41.
23. Yang Y, Liu Y, Yao X, et al. Annexin 1 released by necrotic human glioblastoma cells stimulates tumor cell growth through the formyl peptide receptor 1. Am J Pathol. 2011;179:1504–12.
24. Edwards JG, Cox G, Andi A, et al. Angiogenesis is an independent prognostic factor in malignant mesothelioma. Br J Cancer. 2001;85:863–8.
25. Tan KL, Scott DW, Hong F, et al. tumor-associated macrophages predict inferior outcomes in classic Hodgkin lymphoma: a correlative study from the E2496 Intergroup trial. Blood. 2012;120:3280–7.
26. Iakovlev VV, Gabril M, Dubinski W, et al. Microvascular density as an independent predictor of clinical outcome in renal cell carcinoma: an automated image analysis study. Lab Invest. 2012;92:46–56.

27. Zhang T, Suen CY. A fast parallel algorithm for thinning digital patterns. Commun ACM. 1984;27:236–9.
28. Hlatky L, Hahnfeldt P, Folkman J. Clinical application of antiangiogenic therapy: microvessel density, what it does and doesn't tell us. J Natl Cancer Inst. 2002;94:883–93.
29. Hegi ME, Diserens AC, Gorlia T, et al. MGMT gene silencing and benefit from temozolomide in glioblastoma. N Engl J Med. 2005;352:997–1003.
30. Nabors LB, Portnow J, Ammirati M, et al. Central nervous system cancers, Version 1.2015. J Natl Compr Cancer Netw. 2015;13: 1191–202.
31. Van Meir EG, Hadjipanayis CG, Norden AD, et al. Exciting new advances in neuro-oncology: the avenue to a cure for malignant glioma. Cancer J Clin. 2010;60:166–93.
32. Minniti Gl, Muni R, Lanzetta G, et al. Chemotherapy for glioblastoma: current treatment and future perspectives for cytotoxic and targeted agents. Anticancer Res. 2009;29:5171–84.
33. Louis DN, Perry A, Reifenberger G, et al. The 2016 World Health Organization classification of tumors of the central nervous system: a summary. Acta Neuropathol. 2016;131:803–20.
34. Yan H, Parsons DW, Jin G, et al. IDH1 and IDH2 mutations in gliomas. N Engl J Med. 2009;360:765–73.
35. Zhou Y, Zhou Y, Shingu T, et al. Metabolic alterations in highly tumorigenic glioblastoma cells: preference for hypoxia and high dependency on glycolysis. J Biol Chem. 2011;286:32843–53.
36. Valvona CJ, Fillmore HL, Nunn PB, et al. The regulation and function of lactate dehydrogenase a: therapeutic potential in brain tumor. Brain Pathol. 2016;26:3–17.
37. Helin HO, Tuominen VJ, Ylinen O, et al. Free digital image analysis software helps to resolve equivocal scores in HER2 immunohistochemistry. Virchows Arch. 2016;468:191–8.
38. Konda VJ, Hart J, Lin S, et al. Evaluation of microvascular density in Barrett's associated neoplasia. Mod Pathol. 2013;26: 125–30.
39. Nafe R, Franz K, Schlote W, et al. Morphology of tumor cell nuclei is significantly related with survival time of patients with glioblastomas. Clin Cancer Res. 2005;11:2141–8.
40. Veta M, Kornegoor R, Huisman A, et al. Prognostic value of automatically extracted nuclear morphometric features in whole slide images of male breast cancer. Mod Pathol. 2012;25: 1559–65.
41. Eberhard A, Kahlert S, Goede V, et al. Heterogeneity of angiogenesis and blood vessel maturation in human tumors: implications for antiangiogenic tumor therapies. Cancer Res. 2000;60: 1388–93.
42. Bian XW, Wang QL, Xiao HL, et al. Tumor microvascular architecture phenotype (T-MAP) as a new concept for studies of angiogenesis and oncology. J Neurooncol. 2006;80:211–3.
43. Huang J, Ma X, Chen X, et al. Microvessel density as a prognostic factor in bladder cancer: a systematic review of literature and meta-analysis. Cancer Biomark. 2014;14:505–14.
44. Wyss MT, Hofer S, Hefti M, et al. Spatial heterogeneity of low-grade gliomas at the capillary level: a PET study on tumor blood flow and amino acid uptake. J Nucl Med. 2007;48:1047–52.
45. Goh V, Rodriguez-Justo M, Engledow A, et al. Assessment of the metabolic flow phenotype of primary colorectal cancer: correlations with microvessel density are influenced by the histological scoring method. Eur Radiol. 2012;22:1687–92.
46. Aronen HJ, Pardo FS, Kennedy DN, et al. High microvascular blood volume is associated with high glucose uptake and tumor angiogenesis in human gliomas. Clin Cancer Res. 2000;6: 2189–200.
47. Chinnaiyan P, Kensicki E, Bloom G, et al. The metabolomic signature of malignant glioma reflects accelerated anabolic metabolism. Cancer Res. 2012;72:5878–88.
48. Eramo A, Ricci-Vitiani L, Zeuner A, et al. Chemotherapy resistance of glioblastoma stem cells. Cell Death Differ. 2006;13: 1238–41.
49. Bao S, Wu Q, McLendon RE, et al. Glioma stem cells promote radioresistance by preferential activation of the DNA damage response. Nature. 2006;444:756–60.
50. Tolaney SM, Boucher Y, Duda DG, et al. Role of vascular density and normalization in response to neoadjuvant bevacizumab and chemotherapy in breast cancer patients. Proc Natl Acad Sci USA. 2015;112:14325–30.
51. Zhao YY, Xue C, Jiang W, et al. Predictive value of intratumoral microvascular density in patients with advanced non-small cell lung cancer receiving chemotherapy plus bevacizumab. J Thorac Oncol. 2012;7:71–75.
52. Maheo K, Chevalier S, Vibet S, et al. Non-invasive quantification of tumor vascular architecture during docetaxel-chemotherapy. Breast Cancer Res Treat. 2012;134:1013–25.
53. Rodríguez-Iturbe I, Rinaldo A. Fractal river basins: chance and self-organization. Cambridge, UK: Cambridge University Press, 2001.
54. Warburg O. On the origin of cancer cells. Science. 1956;123: 309–14.
55. Agnihotri S, Zadeh G. Metabolic reprogramming in glioblastoma: the influence of cancer metabolism on epigenetics and unanswered questions. Neuro Oncol. 2016;18:160–72.
56. Saga I, Shibao S, Okubo J, et al. Integrated analysis identifies different metabolic signatures for tumor-initiating cells in a murine glioblastoma model. Neuro Oncol. 2014;16:1048–56.
57. Vander Heiden MG, Cantley LC, Thompson CB. Understanding the Warburg effect: the metabolic requirements of cell proliferation. Science. 2009;324:1029–33.
58. Butler EB, Zhao Y, Munoz-Pinedo C, et al. Stalling the engine of resistance: targeting cancer metabolism to overcome therapeutic resistance. Cancer Res. 2013;73:2709–17.
59. Reishofer G, Koschutnig K, Enzinger C, et al. Fractal dimension and vessel complexity in patients with cerebral arteriovenous malformations. PLoS One. 2012;7:e41148.
60. Camp RL, Dolled-Filhart M, Rimm DL. X-tile: a new bio-informatics tool for biomarker assessment and outcome-based cut-point optimization. Clin Cancer Res. 2004;10:7252–9.